

Interplay of synergy and redundancy in diamond motif

Ayan Biswas* and Suman K Banik†

Department of Chemistry, Bose Institute, 93/1 A P C Road, Kolkata 700 009, India

(Dated: June 21, 2019)

The formalism of partial information decomposition provides independent or non-overlapping components constituting total information content provided by a set of source variables about the target variable. These components are recognised as unique information, synergistic information and, redundant information. The metric of net synergy, conceived as the difference between synergistic and redundant information, is capable of detecting synergy, redundancy and, information independence among stochastic variables. And it can be quantified, as it is done here, using appropriate combinations of different Shannon mutual information terms. Utilisation of such a metric in network motifs with the nodes representing different biochemical species, involved in information sharing, uncovers rich store for interesting results. In the current study, we make use of this formalism to obtain a comprehensive understanding of the relative information processing mechanism in a diamond motif and two of its sub-motifs namely bifurcation and integration motif embedded within the diamond motif. The emerging patterns of synergy and redundancy and their effective contribution towards ensuring high fidelity information transmission are duly compared in the sub-motifs and independent motifs (bifurcation and integration). In this context, the crucial roles played by various time scales and activation coefficients in the network topologies are especially emphasised. We show that the origin of synergy and redundancy in information transmission can be physically justified by decomposing diamond motif into bifurcation and integration motif.

PACS numbers: 87.10.-e, 05.40.-a, 87.18.Tt, 87.18.Vf

I. INTRODUCTION

To optimise different biophysical processes, in continuous and dynamic interactions with their surroundings, animate systems have to perform numerous and necessary computations. The resulting decisions made by the organisms, categorically influence the fitness of the species in the competition for evolutionary selection mechanisms [1–13]. To identify the governing physical principles, that the species are constrained to obey in order to achieve adaptability in a fluctuating environment, sophisticated measures arising from information theory [8, 14, 15] have been proven to be logistically handy as well as predictive [3, 7, 9–11, 16–26]. These optimizing physical principles often dictate the organism in perspective to opt for certain distinctive architectural complexity [1, 27, 28]. The investigation regarding the connection between the topological features of recurrent biological motifs and efficient information processing often costs minimum knowledge of the architectural details of the model system. This is due to the fact that information theory deals with the biological motif as a signal communication system with prominent demarcation for message transmitting source, receiver at the output point and the intermediate signal propagation pathway which one can regard as a black-box. It is this black-box portion where the noise comes in full swing and corrupts the purity of the message which is getting transmitted [14, 29].

Diamond motif (DM) is one of the recurring biological patterns [27, 30, 31], which is interesting on a num-

ber of counts. It is one of the two prominent four node motifs found in signal transduction networks, the other being the bi-fan. Surprisingly, DM (initially known as Bi-parallel [27]) is found to occur in diverse networks e.g., in neuronal networks of *C. elegans*, ecological food webs and in forward logic chips embedded in electronic circuits [27, 30, 31]. DM is able to be generalised as multiple layered perceptrons also found in the neural network of *C. elegans*. One can decompose the DM into combinations of various sub-motifs and discuss the arising advantage points. We know one such prominent attempt using information-theoretic analysis where the authors have methodically dissected the DM into two two-step cascade motifs and characterised profiles of gain, noise and the gain-to-noise ratio [32]. In that paper, the evocation of DM comes in the perspective of multimerisation and the analysis shows the emergence of a band-pass filter type behaviour of DM. One of the key conclusions rendered in that piece of work, suggests that network performance is independent of its architectural features and can be manipulated by modification of inter-species coupling strengths. Another approach has identified DM as a generalisation of incoherent feed-forward loop motif and the results obtained also show its band-pass filter type response to signal with temporal periodicity [33]. In the present communication, however, we have looked into the problem of efficient information processing in the DM from a fresh perspective. One can think of constructing DM using independent bifurcation motif (BM) and independent integration motif (IM) whereas it is also possible to identify two different sub-motifs embedded in DM, namely bifurcation sub-motif (BM-DM) and integration sub-motif (IM-DM) (see Fig. 1).

We have adopted an information-theoretic measure

* ayanbiswas@jcbosc.ac.in

† skbanik@jcbosc.ac.in

which involves a suitable combination of three-variable and two-variable mutual information (MI) terms, so that the combination known as the net synergy [34, 35], can have the potential to predict synergy, redundancy and, information independence among stochastic variables involved in information processing in a specified system. The metric of net synergy is an important product of partial information decomposition (PID) [35, 36]. Using PID, one can decompose total information provided by a set of source variables about a target variable, into a number of independent or non-overlapping information terms namely unique information, synergistic information and, redundant information. Unique information is the information about the target variable provided only by a specific source variable whereas redundant information about the target is provided by all the source variables holding common shares. The remaining candidate i.e., synergistic information about the target is provided jointly by the set of source variables. In other words, to get hold of the synergistic information about a target variable, one has to know all the source variables simultaneously. In this formalism, the net synergy is defined as the difference between synergistic information and redundant information [35]. If the net synergy is positive valued, it is implied that synergy is dominant over redundancy whereas, for negative values of the net synergy, redundancy overpowers synergy. The borderline case of zero net synergy indicates information independence among information source and target variables [34, 35].

There exists a considerably rich literature on multivariate information decomposition. In a broader perspective, Faes *et. al.*, have been able to show that computation of information storage and its transfer are necessary to predict the dynamics of target variable [37]. Apart from information storage and transfer, Ref. 38, directs our attention to assemble information modification formalism to better understand dynamics of complex network topologies. Besides, composite analysis of information-dynamic measures can underpin the causal effects that follow from the dynamics which itself is susceptible to varying experimental conditions [39]. In a study performed by Bertschinger *et. al.*, measures have been proposed for decompositions of multivariate MI-s along with a working concept for the unique information [40]. Different quantifiers of synergistic information have been applied in a set of binary circuits for their comparative analysis [41]. For a new formalism regarding redundant information and its usage to decompose transfer entropy, one can take note of the proposal by Harder *et. al.*, [42]. Recent findings according to Wibral and colleagues, have projected PID as a consistent framework such that it can efficiently compare different neural goal functions and formulate potential new candidates [43]. To supplement advances in theoretical understanding on multivariate information decomposition, experimentalists have also contributed their fair share in this ever growing research domain. Gawne and Richmond

have done an excellent experimental work exploring synergistic, redundant and, independent information encoding inside the inferior temporal cortex region in behaving rhesus monkey brain [44]. The role played by correlations in the encoding mechanisms inside the nervous system has also been central to elaborate and thought provoking research [45]. In the work of Brenner *et. al.*, it has been demonstrated that even the visual information processing device of a fly, consisting neuron which is sensitive towards motion generated stimulus, uses synergistic code [46].

The role of redundancy in combating noise in the information propagation channel was previously presented by Shannon and Weaver in their illuminating book [47] which further motivated us to look into this matter in the context of model network motifs. The theoretical explanation regarding origin of redundancy in a two-step cascade motif and its connection with information fidelity have been discussed thoroughly in our earlier work [48]. In Ref. 49, authors have presented a case of redundancy where multiple genes with successively higher values of activating signal strengths, are driven by a single input. Another interesting recent study has found out that genetic redundancy along with intrinsic noise and heterogeneity can increase information transfer whereas extrinsic noise and cross-talk have an inverse effect [50]. Immunofluorescence readouts from network experiments involving NF- κ B and ATF-2, receiving signal from tumor necrosis factor (TNF) through TNF receptor, reveal mitigation of noisy effects and consequent increase in information propagation with the help of redundancy [21]. Rhee and colleagues have been successful in detecting connections between network architecture and associated noise of biochemical origin [51]. Whereas these studies have reported the connection between information fidelity and redundancy (architectural or/and informational), our analysis has quantified this connection in model network motif with a fresh information-theoretic point of view. Moreover in our current initiative, attempts have been made to showcase the connection between network topology and the synergy-redundancy duo. And to be specific, this line of analysis qualifies for being the central theme of the present report.

To this end, we have chosen signal-to-noise ratio (SNR) as the measure of fidelity [24, 48] in the DM. Gain-to-noise ratio (GNR) plays another strong candidate which can successfully quantitate the performance of the network motif and it does so independent of the signal characteristics [20]. One can also link GNR to the Fisher information about the signalling species provided by the output species forming the response [15, 20]. The analysis performed here has been done at steady states of involved species as it is suggested that living systems perform optimally in their steady states and keeping concentrations or copy numbers fixed helps to compare different parametric scenarios on an equal footing [30]. Additionally since in our case, the signalling species driving the DM follows poisson process, SNR is found to be propor-

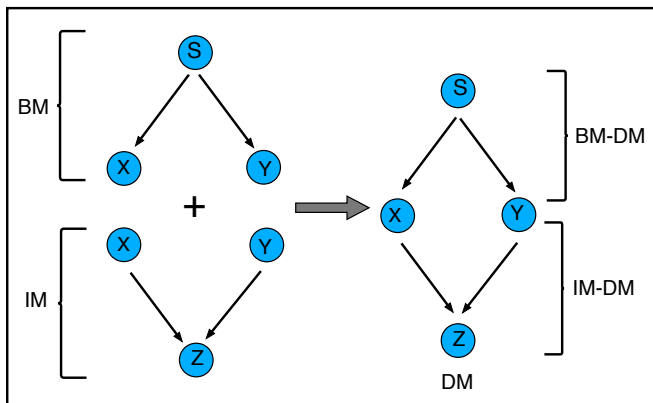


FIG. 1. Schematic diagram of bifurcation motif (BM), integration motif (IM) and diamond motif (DM). BM-DM and IM-DM stand for the bifurcation and integration sub-motif embedded within the diamond motif.

tional to GNR. Here, the steady state ensemble averaged population of the signalling species serves as the constant factor of proportionality.

The objective to use relaxation time scale as a variation parameter is to take benefit of the fact that separation of time scale is indeed a crucial factor that dictates how information can flow in a biochemical network behaving like a noise filter [13, 20, 32, 52–54]. Some other technical points that the present report takes benefits of are as follows. We have used Gaussian random variables to represent the biochemical species so that we can treat the MI of various channels as their respective channel capacities [20] and these can be easily computed using corresponding variance and covariance. We have made our analysis tractable further by assuming Gaussian noise processes [4, 18, 20, 48, 52, 54–59]. We are justified enough using noise with zero cross-correlation, because biological phenomenology dictates validity of this approach in a birth-death type of dynamics [32], as dealt here. Another important point to note here is the consideration of low copy number [4, 6, 49, 60, 61] of the biochemical species involved in the stochastic reactions.

The theoretical analysis performed in this paper makes use of linear noise approximation (LNA) [55, 56, 59, 62–64] to handle nonlinearity which enters into the system through the Hill type regulatory functions [18, 49, 65–67] used in our model system. And we do take note of the fact that there are other techniques e.g., the small-noise approximation that can be applied to tackle the fluctuations in the system [49, 68]. Though low copy numbers of the reacting molecules contribute a significant amount of noise into the reaction volume, a good match between our analytical results and stochastic simulations based on Gillespie’s method [69, 70] establishes the validity of LNA. And in this connection, our observations receive strong support from previous findings of similar type considering copy number as low as ~ 10 [18, 48, 52, 54]. From current literature [59], LNA is known to be effective

beyond the cases of high copy number reactions. It gives exact results up to the second moments of the system components involved in second-order reactions. There may be a number of species that are involved in these specific type of reactions but it is noted that at least one of those reacting species in every such reaction fluctuates not only in a Poissonian way but also in an uncorrelated fashion with the rest of the species [59].

II. THE MODEL

The set of Langevin equations governing the dynamics of a DM are,

$$\frac{ds}{dt} = f_s(s) - \mu_s s + \xi_s(t), \quad (1)$$

$$\frac{dx}{dt} = f_x(s, x) - \mu_x x + \xi_x(t), \quad (2)$$

$$\frac{dy}{dt} = f_y(s, y) - \mu_y y + \xi_y(t), \quad (3)$$

$$\frac{dz}{dt} = f_z(s, x, y, z) - \mu_z z + \xi_z(t). \quad (4)$$

Here, to represent the copy numbers of species S, X, Y and Z in the unit amount of cellular volume, we use the symbols s, x, y and z , respectively. To be precise, if one considers these biochemical species to be transcription factors, the corresponding volume has to be an effective volume since these transcription factors after being produced in the cytoplasm are carried inside the nucleus where they are sensed. Hence merely considering either the cellular or the nuclear volume would be inaccurate [67]. The set of Langevin equations written above is suggestive of birth-death type of mechanisms governing the population levels. We have modelled degradation to be proportional to the respective population size with μ_i -s ($i = s, x, y, z$) setting the time scale of degradation. The inter-species interactions are manifested through the synthesis of X, Y and Z. These terms are taken to be non-linear in general in agreement with real biological scenario [18, 32, 65, 66, 68]. In the present analysis we use $\langle \xi_i(t) \rangle = 0$ and $\langle \xi_i(t) \xi_j(t') \rangle = \langle |\xi_i|^2 \rangle \delta_{ij} \delta(t - t')$, which makes the noise processes independent and Gaussian distributed. At steady state the noise strength becomes $\langle |\xi_i|^2 \rangle = \langle f_i \rangle + \mu_i \langle i \rangle = 2\mu_i \langle i \rangle$ where $i = s, x, y$ and z [55–57, 61–63, 71, 72]. The first equality demonstrates the fact that both synthesis and degradation processes are sources for noise in the system and their individual contributions add up to produce the ultimate steady state noise strength. The second equality indicates at steady state, both the noise sources contribute in equal proportions. The usage of $\langle \dots \rangle$ denotes steady state ensemble average over many independent realisations. To calculate the second moments of s, x, y and z through LNA, we apply perturbation of linear order $\delta u(t) = u(t) - \langle u \rangle$ with $\langle u \rangle$ being the average population of u at steady state and

recast Eqs. (1-4) in the following form

$$\frac{d\delta\mathbf{W}}{dt} = \mathbf{J}_{W=\langle W \rangle} \delta\mathbf{W}(t) + \Xi(t), \quad (5)$$

where we denote by $\delta\mathbf{W}(t)$, the fluctuations matrix containing the linear order perturbations and the noise matrix by $\Xi(t)$

$$\delta\mathbf{W}(t) = \begin{pmatrix} \delta s(t) \\ \delta x(t) \\ \delta y(t) \\ \delta z(t) \end{pmatrix}, \Xi(t) = \begin{pmatrix} \xi_s(t) \\ \xi_x(t) \\ \xi_y(t) \\ \xi_z(t) \end{pmatrix}.$$

\mathbf{J} represents the Jacobian matrix at steady state. The Lyapunov equation at steady state [61–63, 73, 74]

$$\mathbf{J}\Sigma + \Sigma\mathbf{J}^T + \mathbf{D} = \mathbf{0}, \quad (6)$$

establishes connections between the steady state fluctuations of the biochemical species and noise driven dissipation in the system. The fluctuations part is encapsulated in Σ which is the covariance matrix and \mathbf{D} contains the dissipation part since its entries are various noise strengths, i.e., $\mathbf{D} = \langle \Xi\Xi^T \rangle$ where T denotes matrix transposition operation.

In the generalized analytic expressions of the second moments (see Appendix), obtained by solving the Lyapunov equation at steady state, s, x, y and, z are approximated as $\langle s \rangle, \langle x \rangle, \langle y \rangle$ and, $\langle z \rangle$, respectively [48, 54, 55]. These second moments serve as the ingredients for calculating the two-variable and three-variable MI terms. For computing the net synergy (in the unit of ‘bits’) among S, X and, Y which constitute BM and BM-DM, and among X, Y and, Z which constitute IM and IM-DM, we use the following two expressions [26, 34–36, 48]

$$\Delta I(s; x, y) = I(s; x, y) - I(s; x) - I(s; y), \quad (7)$$

$$\Delta I(z; x, y) = I(z; x, y) - I(z; x) - I(z; y). \quad (8)$$

We reiterate here that positive net synergy ($\Delta I > 0$) reveals a greater amount of synergy in comparison with redundancy while negative net synergy ($\Delta I < 0$) reverses the situation. Synergy and redundancy can also balance each other and this gets reflected in zero amount of the net synergy ($\Delta I = 0$). For Gaussian random variables, Eqs. (7-8) become [35]

$$\Delta I(s; x, y) = \frac{1}{2} \left(\log_2 \left[\frac{\det \Sigma(s)}{\det \Sigma(s|x, y)} \right] - \log_2 \left[\frac{\det \Sigma(s)}{\det \Sigma(s|x)} \right] - \log_2 \left[\frac{\det \Sigma(s)}{\det \Sigma(s|y)} \right] \right), \quad (9)$$

$$\Delta I(z; x, y) = \frac{1}{2} \left(\log_2 \left[\frac{\det \Sigma(z)}{\det \Sigma(z|x, y)} \right] - \log_2 \left[\frac{\det \Sigma(z)}{\det \Sigma(z|x)} \right] - \log_2 \left[\frac{\det \Sigma(z)}{\det \Sigma(z|y)} \right] \right). \quad (10)$$

The consecutive terms in the right hand side of Eq. (9) denote $I(s; x, y)$, $I(s; x)$ and, $I(s; y)$, respectively. Similarly, the consecutive terms in the right hand side of

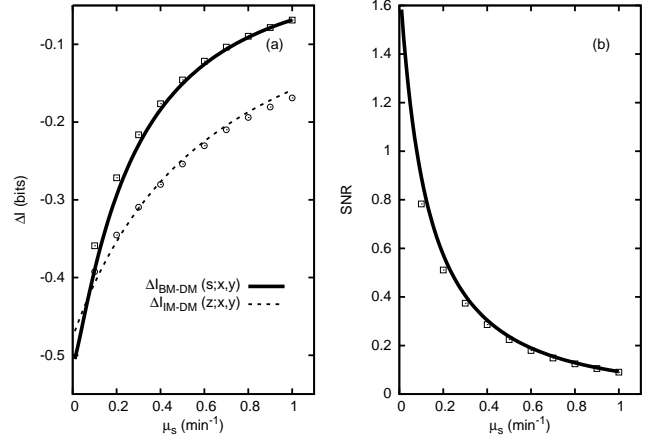


FIG. 2. (a) The net synergy for BM-DM ($\Delta I_{BM-DM}(s; x, y)$) and for IM-DM ($\Delta I_{IM-DM}(z; x, y)$) and, (b) SNR as functions of μ_s . The lines are due to analytical results and the symbols represent numerical data generated using Gillespie’s algorithm [69, 70] with ensemble averaging over 10^9 independent time series. The constraint relations for species populations are $\langle s \rangle = 10$, $\langle x \rangle = 100$, $\langle y \rangle = 100$ and, $\langle z \rangle = 100$. The rate parameters relevant for BM-DM and IM-DM are $k_s = \mu_s \langle s \rangle$, $k_x = \mu_x \langle x \rangle ((K_1^n + \langle s \rangle^n) / \langle s \rangle^n)$, $k_y = \mu_y \langle y \rangle ((K_2^n + \langle s \rangle^n) / \langle s \rangle^n)$ and, $k_z = \mu_z \langle z \rangle ((K_3^n + \langle x \rangle^n) / \langle x \rangle^n) ((K_4^n + \langle y \rangle^n) / \langle y \rangle^n)$. $K_1 = K_2 = 10$, $K_3 = K_4 = 100$, $\mu_x = \mu_y = 0.5 \text{ min}^{-1}$, $\mu_z = 5 \text{ min}^{-1}$. In both the cases, we have used $n = 1$.

Eq. (10) denote $I(z; x, y)$, $I(z; x)$ and, $I(z; y)$, respectively. The terms appearing in the denominators of the MI-s present in Eqs. (9,10) are the corresponding conditional variances and can be computed as follows [35]

$$\Sigma(s|x) =: \Sigma(s) - \Sigma(s, x) [\Sigma(x)]^{-1} \Sigma(x, s), \quad (11)$$

$$\Sigma(s|y) =: \Sigma(s) - \Sigma(s, y) [\Sigma(y)]^{-1} \Sigma(y, s), \quad (12)$$

$$\Sigma(s|x, y) =: \Sigma(s) - \begin{pmatrix} \Sigma(s, x) & \Sigma(s, y) \end{pmatrix} \begin{pmatrix} \Sigma(x) & \Sigma(x, y) \\ \Sigma(y, x) & \Sigma(y) \end{pmatrix}^{-1} \begin{pmatrix} \Sigma(x, s) \\ \Sigma(y, s) \end{pmatrix} \quad (13)$$

We note that, the covariances are symmetric e.g., $\Sigma(s, x) = \Sigma(x, s)$ etc. In a similar fashion, one can compute necessary expressions involving x, y , and, z . For explicit generalized forms of the variance and covariance, we refer to the Appendix.

III. RESULTS AND DISCUSSION

As mentioned in the introduction, in the present report, we aim to quantify information transmission in terms of the net synergy in the DM and to do so efficiently, we have identified two sub-motifs namely the BM-DM and the IM-DM, embedded within the DM (Fig. 1). The net synergy is explored in the independent BM and IM (Fig. 1) and also when both the motifs are ingrained in the DM as sub-motifs. This has

been done to quantify the dependance of DM on two of its sub-motifs in the context of information processing and mitigation of noise. Fig. 2(a,b) shows the net synergy $\Delta I_{BM-DM}(s; x, y)$ and $\Delta I_{IM-DM}(z; x, y)$ for BM-DM and IM-DM, respectively, along with the SNR as a function of μ_s with $\mu_x = \mu_y = 0.5 \text{ min}^{-1}$ and $\mu_z = 5 \text{ min}^{-1}$. To check the validity of our analytical calculations, we also execute the numerical simulation of the kinetics (see Table I) following stochastic simulation algorithm [69, 70]. In both the analytical and numerical calculations, we keep the species population fixed e.g., $\langle s \rangle = 10$, $\langle x \rangle = 100$, $\langle y \rangle = 100$ and, $\langle z \rangle = 100$, irrespective of the network architecture examined. This strategy has the advantage of comparing the optimal performances of species at steady state at par with each other [30]. The constraint of population constancy governs choices of the synthesis rate parameters while one can make independent choices for the degradation rate parameters. For example, in the BM $k_s = \mu_s \langle s \rangle$, $k_x = \mu_x \langle x \rangle ((K_1^n + \langle s \rangle^n) / \langle s \rangle^n)$, and, $k_y = \mu_y \langle y \rangle ((K_2^n + \langle s \rangle^n) / \langle s \rangle^n)$. Similarly for the IM we use, $k_x = \mu_x \langle x \rangle$, $k_y = \mu_y \langle y \rangle$ and, $k_z = \mu_z \langle z \rangle ((K_3^n + \langle x \rangle^n) / \langle x \rangle^n) ((K_4^n + \langle y \rangle^n) / \langle y \rangle^n)$. Finally for the DM the synthesis rate parameters are as follows, $k_s = \mu_s \langle s \rangle$, $k_x = \mu_x \langle x \rangle ((K_1^n + \langle s \rangle^n) / \langle s \rangle^n)$, $k_y = \mu_y \langle y \rangle ((K_2^n + \langle s \rangle^n) / \langle s \rangle^n)$ and, $k_z = \mu_z \langle z \rangle ((K_3^n + \langle x \rangle^n) / \langle x \rangle^n) ((K_4^n + \langle y \rangle^n) / \langle y \rangle^n)$. We note that while generating profiles (analytical and numerical) in Fig. 2, we have used $n = 1$. The net synergy profiles are constrained in the negative domain and show a hyperbolic trend with increasing μ_s thereby lowering the level of redundancy. Here, redundancy takes care of common information sharing among the nodes of the diamond motif - a signature of PID. The collateral investigation on SNR, calculated taking S as the signal and Z as the response, shows opposite trend thereby suggesting that redundancy enhances the fidelity of the signalling pathway [48]. The observed agreement between the analytical and numerical results are indicative of the effectiveness of LNA applied in our calculation which adopts the set of copy numbers consisting $\langle s \rangle = 10$, $\langle x \rangle = 100$, $\langle y \rangle = 100$ and, $\langle z \rangle = 100$ [18, 48, 52, 54].

The two maps in Fig. 3(a,b) are generated through scanning the parameter spaces of μ_x and μ_y for fixed signal relaxation rate $\mu_s = 0.1 \text{ min}^{-1}$ and depict the net synergy $\Delta I_{BM}(s; x, y)$ and $\Delta I_{BM-DM}(s; x, y)$ of BM and BM-DM, respectively. Fig. 4(a,b) do the same for $\mu_s = 1 \text{ min}^{-1}$. The maps of the net synergy $\Delta I_{IM}(z; x, y)$ and $\Delta I_{IM-DM}(z; x, y)$ of IM and IM-DM, respectively, are also shown in Fig. 3(c,d) and Fig. 4(c,d) for $\mu_s = 0.1 \text{ min}^{-1}$ and $\mu_s = 1 \text{ min}^{-1}$, respectively. Qualitatively comparing the panels in Fig. 3(a,b) and Fig. 4(a,b), it is observed that $\Delta I_{BM}(s; x, y) = \Delta I_{BM-DM}(s; x, y)$. This result shows that the bifurcation motif after getting embedded within the DM acts independent of the integration sub-motif to carry out information transmission and this fact holds without any regard for variations in μ_s . But this is not the case in the signal integration scenario. Fig. 3(c) shows positive net syn-

TABLE I. Table of the chemical reactions and associated propensities for the diamond motif. Here, S, X, Y and, Z stand for biochemical species and s, x, y and, z represent copy numbers of the respective species expressed in molecules/ V with V being the unit effective cellular volume. For X and Y mediated production of Z, an AND gate is used to integrate individual contributions from the synthesising species. We have taken Hill coefficient $n = 1$. The unit of corresponding rate constants is min^{-1} .

Biochemical Processes	Reaction	Propensity
Synthesis of S	$\phi \rightarrow S$	k_s
Degradation of S	$S \rightarrow \phi$	$\mu_s s$
S mediated synthesis of X	$S \rightarrow S + X$	$k_x \frac{s^n}{K_1^n + s^n}$
Degradation of X	$X \rightarrow \phi$	$\mu_x x$
S mediated synthesis of Y	$S \rightarrow S + Y$	$k_y \frac{s^n}{K_2^n + s^n}$
Degradation of Y	$Y \rightarrow \phi$	$\mu_y y$
X and Y mediated synthesis of Z	$X + Y \rightarrow X + Y + Z$	$k_z \frac{x^n}{K_3^n + x^n} \frac{y^n}{K_4^n + y^n}$
Degradation of Z	$Z \rightarrow \phi$	$\mu_z z$

ergy $\Delta I_{IM}(z; x, y)$ spanning the entire parameter range whereas Fig. 3(d) shows redundancy in abundance since most of the net synergy profile $\Delta I_{IM-DM}(z; x, y)$ is in the negative domain only with a miniscule positive valued region. Fig. 4(a,d) shows reduced amount of redundancy in comparison with their corresponding counterparts in Fig. 3. Since species S is not a part of the IM, changing μ_s does not alter the fabric of its net synergy as shown in Figs. 3(c) and 4(c) and by looking at these profiles it is confirmed that $\Delta I_{IM}(z; x, y)$ (for $\mu_s = 0.1 \text{ min}^{-1}$) = $\Delta I_{IM}(z; x, y)$ (for $\mu_s = 1 \text{ min}^{-1}$).

To comprehend the nature of the net synergy profiles, we take note of the fact that there are multiple time scales involved with the biochemical species constituting different topologies (BM, BM-DM, IM, IM-DM and, DM). These time scales play crucial roles to affect the information flow along the motif sometimes facilitating propagation of information and hindering otherwise [32, 52–54]. Now, we re-express the preceding statement as a guiding principle to analyse information flow in the motif under investigation. Whenever the upstream species concentration fluctuates slowly as compared to its immediate downstream species i.e., the upstream species has got a relatively small relaxation rate with respect to that of the downstream species, it helps the downstream species to sense the upstream fluctuations accurately thereby allowing information flow to occur. In the opposite scenario, the downstream species fails to follow the rapid upstream fluctuations with adequate precision thereby obstructing the information propagation. In both the cases mentioned, the corresponding effects get pronounced depend-

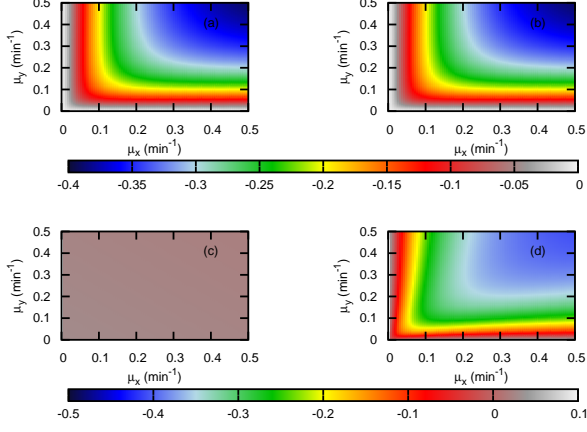


FIG. 3. Theoretical profiles (a)-(b) show variations in $\Delta I_{BM}(s; x, y)$ and $\Delta I_{BM-DM}(s; x, y)$ measured in bits as functions of μ_x and μ_y , respectively. Similarly, (c)-(d) show variations in $\Delta I_{IM}(z; x, y)$ and $\Delta I_{IM-DM}(z; x, y)$ measured in bits as functions of μ_x and μ_y , respectively. These maps are generated keeping $\mu_s = 0.1 \text{ min}^{-1}$ and $\mu_z = 5 \text{ min}^{-1}$. The synthesis rate parameters for BM are $k_s = \mu_s \langle s \rangle$, $k_x = \mu_x \langle x \rangle ((K_1^n + \langle s \rangle^n) / \langle s \rangle^n)$ and, $k_y = \mu_y \langle y \rangle ((K_2^n + \langle s \rangle^n) / \langle s \rangle^n)$. For IM the synthesis rates are $k_x = \mu_x \langle x \rangle$, $k_y = \mu_y \langle y \rangle$ and, $k_z = \mu_z \langle z \rangle ((K_3^n + \langle x \rangle^n) / \langle x \rangle^n) ((K_4^n + \langle y \rangle^n) / \langle y \rangle^n)$. The synthesis rate parameters associated with DM are $k_s = \mu_s \langle s \rangle$, $k_x = \mu_x \langle x \rangle ((K_1^n + \langle s \rangle^n) / \langle s \rangle^n)$, $k_y = \mu_y \langle y \rangle ((K_2^n + \langle s \rangle^n) / \langle s \rangle^n)$ and, $k_z = \mu_z \langle z \rangle ((K_3^n + \langle x \rangle^n) / \langle x \rangle^n) ((K_4^n + \langle y \rangle^n) / \langle y \rangle^n)$. We maintain $\langle s \rangle = 10$, $\langle x \rangle = 100$, $\langle y \rangle = 100$, $\langle z \rangle = 100$, $K_1 = K_2 = 10$, $K_3 = K_4 = 100$ and, $n = 1$.

ing upon how distantly are these time scales separated with respect to each other [54].

The net synergy profiles in Fig. 2(a) can be well understood keeping the above mentioned principle in perspective. The range of variation of μ_s spans regions with $\mu_s < \mu_x(\mu_y)$, $\mu_s = \mu_x(\mu_y)$ and $\mu_s > \mu_x(\mu_y)$. At the same time, by keeping $\mu_z = 5 \text{ min}^{-1}$ which is 10 times faster than $\mu_x(\mu_y)$, fixed at 0.5 min^{-1} , adequate amount of information flow is allowed for convenience. It is clear from Fig. 2(a) that as the source species fluctuates faster compared to downstream species, transmitted amount of redundant information decreases.

In Fig. 3(a), as we move along the diagonal from low $\mu_x(\mu_y)$ to high $\mu_x(\mu_y)$, it is observed that the value of net synergy $\Delta I_{BM}(s; x, y)$ becomes more negative implying increase in redundancy. It should be noted that moving along this diagonal direction, both the downstream species X and Y become more sensitive towards the signal (S) fluctuations thereby able to harness more information. By this token, the amount of common or redundant information content between X and Y about S increases causing the net synergy to decrease.

One can compare the situations of BM in Figs. 3(a) and 4(a) subject to variation in the signal relaxation. It is clearly visible that with increased μ_s from 0.1 min^{-1} to 1 min^{-1} the domain of net synergy shifts close to zero

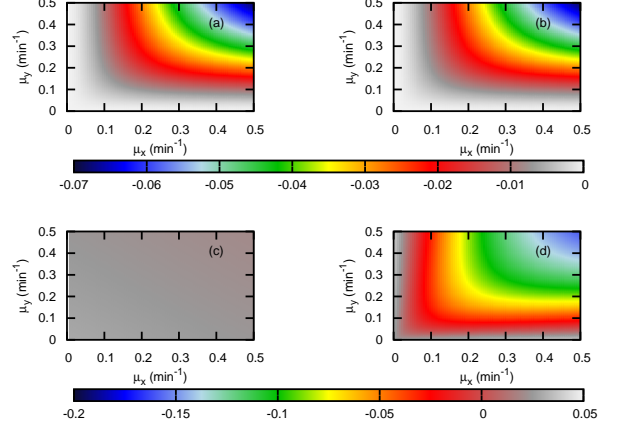


FIG. 4. Theoretical profiles (a)-(b) show variations in $\Delta I_{BM}(s; x, y)$ and $\Delta I_{BM-DM}(s; x, y)$ measured in bits as functions of μ_x and μ_y , respectively. Similarly, (c)-(d) show variations in $\Delta I_{IM}(z; x, y)$ and $\Delta I_{IM-DM}(z; x, y)$ measured in bits as functions of μ_x and μ_y , respectively. These maps are generated keeping $\mu_s = 1 \text{ min}^{-1}$ and $\mu_z = 5 \text{ min}^{-1}$. The synthesis rate parameters for BM are as follows. $k_s = \mu_s \langle s \rangle$, $k_x = \mu_x \langle x \rangle ((K_1^n + \langle s \rangle^n) / \langle s \rangle^n)$ and, $k_y = \mu_y \langle y \rangle ((K_2^n + \langle s \rangle^n) / \langle s \rangle^n)$. For IM these are $k_x = \mu_x \langle x \rangle$, $k_y = \mu_y \langle y \rangle$ and, $k_z = \mu_z \langle z \rangle ((K_3^n + \langle x \rangle^n) / \langle x \rangle^n) ((K_4^n + \langle y \rangle^n) / \langle y \rangle^n)$. The corresponding set for DM is as follows. $k_s = \mu_s \langle s \rangle$, $k_x = \mu_x \langle x \rangle ((K_1^n + \langle s \rangle^n) / \langle s \rangle^n)$, $k_y = \mu_y \langle y \rangle ((K_2^n + \langle s \rangle^n) / \langle s \rangle^n)$ and, $k_z = \mu_z \langle z \rangle ((K_3^n + \langle x \rangle^n) / \langle x \rangle^n) ((K_4^n + \langle y \rangle^n) / \langle y \rangle^n)$. We maintain $\langle s \rangle = 10$, $\langle x \rangle = 100$, $\langle y \rangle = 100$, $\langle z \rangle = 100$, $K_1 = K_2 = 10$, $K_3 = K_4 = 100$ and, $n = 1$.

value. Such change in the nature of the net synergy profile is due to the fact that in Fig. 4(a) fixing $\mu_s = 1 \text{ min}^{-1}$ blocks information flow significantly in the motif since both the downstream species X and Y fluctuates in the range of $0 - 0.5 \text{ min}^{-1}$, slower than the time scale of fluctuations of the source species S.

In Fig. 3(c), the net synergy $\Delta I_{IM}(z; x, y)$ is entirely constrained in the positive domain. Since we have not specified synergy and redundancy independently in a quantitative manner, we are not certain that whether this positive nature is due to pure synergy or synergy being dominant over redundancy but we can at least make a guess work based on intuition. Redundancy being sharing of information [35], may originate from a common source which in this case (i.e., IM) is absent. There are two uncorrelated source X and Y and single target Z in IM unlike in BM where the target X and Y shares a common source S. Absence of a common source is suggestive of pure synergy over the entire parameter space (Figs. 3(c) and 4(c)). However, in Figs. 3(d) and 4(d), the net synergy decreases along the diagonal from low $\mu_x(\mu_y)$ to high $\mu_x(\mu_y)$ which is at par with the previously placed argument based on the idea of separation of time scales.

The four edges of DM are characterised by three types of parameters namely the activation coefficients

(K_1, K_2, K_3 and K_4), the synthesis rates of biochemical species (k_s, k_x, k_y and k_z) and the Hill coefficient (n) of the input regulatory functions. This minimal set of parameters ($K_1, K_2, K_3, K_4, k_s, k_x, k_y, k_z$ and n) can be tuned during simple evolution experiments performed in the laboratory. It has been argued that in a dynamically changing environment, these parameters associated with the population of each of the biochemical species, encounter selection pressure and thus precisely optimise the expression levels [30]. The time scale of their adaptability is typically of the order of hundred of generations. Experimentally, K_i ($i = 1, 2, 3, 4$) can be altered by inducing mutations in the DNA sequences of the promoter region where the activating/repressing molecules bind. To do alteration in k_i ($i = s, x, y, z$), the binding site sequence for RNA polymerase complex, are mutated. If suitable parameterization of motifs is done with these numbers, then experiments can be designed to place the biological motifs under selection pressure. Uri Alon goes on to point out that the resulting changes, an organism acquire under such pressure, are inheritable through generations facing changing environmental conditions [30]. These phenomenological inputs motivate us to link information processing with these numbers. In the previous figures, we have already done so by varying μ_i ($i = s, x, y, z$), thereby making variations in k_i ($i = s, x, y, z$) since the constraint of fixed population size at steady state, makes $k_i \propto \mu_i$ ($i = s, x, y, z$). We further reiterate that in our calculation we have used $n = 1$ to retain the level of nonlinearity in the input regulatory functions tractable analytically under the purview of LNA.

Figure 5(a,b) portrays the effect of variations of K_1, K_2, K_3 and K_4 on the net synergy $\Delta I_{BM-DM}(s; x, y)$ and $\Delta I_{IM-DM}(z; x, y)$, respectively. We have kept $\mu_s = 0.1 \text{ min}^{-1}$, $\mu_x = \mu_y = 0.5 \text{ min}^{-1}$, $\mu_z = 5 \text{ min}^{-1}$ to show the above mentioned variations subject to the constraint $K_1 = K_2$ and $K_3 = K_4$. By making such set of arrangements, we have ensured adequate information flow in the motif while keeping architectural redundancy (based on interactions) in between both the bifurcating and the integrating branches. Figure 5(a) shows that the net synergy $\Delta I_{BM-DM}(s; x, y)$ is not responsive of changes in K_3 and K_4 , reaffirming the fact that the information flow in the integration sub-motif does not alter anyway the information processing in the upper-level topology i.e., the bifurcation sub-motif. This figure also indicates that with increasing $K_1(K_2)$, redundancy contributes more, making the net synergy more negative. Similarly in Fig. 5(b), we show that at the high end of $K_1(K_2)$, the two integrating branches of the diamond motif, contribute the maximum level of redundancy in the entire map. This map also implies that $\Delta I_{IM-DM}(z; x, y)$ is nearly insensitive towards variations in $K_3(K_4)$. Here, the intermediate information sources X and Y which are activated by the source S from low to moderate strength, can not influence significantly the target Z by modulating $K_3(K_4)$. In this respect, we restate that the strength of activation is determined by the parameters K_1, K_2, K_3

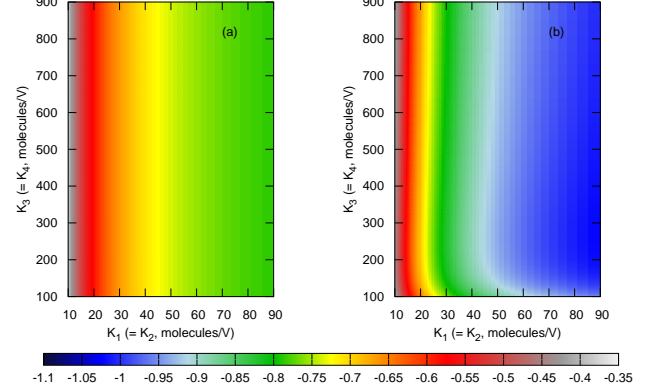


FIG. 5. The 2d maps (a),(b) portray $\Delta I_{BM-DM}(s; x, y)$ and $\Delta I_{IM-DM}(z; x, y)$ as functions of $K_1(= K_2)$ and $K_3(= K_4)$ respectively, in the unit of bits. The populations of the biochemical species S, X, Y and, Z are fixed at steady state $\langle s \rangle = 10$, $\langle x \rangle = 100$, $\langle y \rangle = 100$ and, $\langle z \rangle = 100$. The relevant rate parameters are $k_s = \mu_s \langle s \rangle$, $k_x = \mu_x \langle x \rangle ((K_1^n + \langle s \rangle^n) / \langle s \rangle^n)$, $k_y = \mu_y \langle y \rangle ((K_2^n + \langle s \rangle^n) / \langle s \rangle^n)$ and, $k_z = \mu_z \langle z \rangle ((K_3^n + \langle x \rangle^n) / \langle x \rangle^n) ((K_4^n + \langle y \rangle^n) / \langle y \rangle^n)$. We use $\mu_s = 0.1 \text{ min}^{-1}$, $\mu_x = \mu_y = 0.5 \text{ min}^{-1}$, $\mu_z = 5 \text{ min}^{-1}$ and, $n = 1$ to generate the theoretical figures.

and, K_4 . To be specific, by using $K_1 = K_2 = 10 - 90$ and $K_3 = K_4 = 100 - 900$, the nonlinear regulatory functions ($s^n / (K_1^n + s^n)$, $s^n / (K_2^n + s^n)$, $x^n / (K_3^n + x^n)$ and, $y^n / (K_4^n + y^n)$) in the production terms for X, Y and, Z, respectively, take numerical values in the range of 0.1 (weak activation)–0.5 (moderate activation) at steady state. The maps in Fig. 5(a,b) show that, with decreasing strength of activation of the intermediate X and Y, the system acquires more redundancy both for the BM-DM and the IM-DM. Here we redirect our attention to Fig. 2(a,b) where we have observed redundancy increases with SNR which plays the metric for fidelity in information processing [24]. Keeping these points in our perspective, we propose that under weak activation levels (i.e., for low values of the nonlinear terms $s^n / (K_1^n + s^n)$, etc.) evolution will apply selection pressure (by incorporating suitable mutations) such that noise minimising biological motifs will eventually favour regulation of biochemical species X and Y acting as information generating hubs.

To capture how the bifurcation and integration sub-motifs perform relative to each other in terms of their individual net synergy contributions, we show $\Delta I_{IM-DM}(z; x, y) - \Delta I_{BM-DM}(s; x, y)$ as a function of μ_x and μ_y for $\mu_s = 0.1 \text{ min}^{-1}$, $\mu_s = 0.5 \text{ min}^{-1}$ and, $\mu_s = 1 \text{ min}^{-1}$ in Fig. 6(a-c), respectively. The bifurcation sub-motif dominates in all of these landscapes which are negatively valued in most of the parts. The domain with maximum negativity, shifts higher up the diagonal ($\mu_x = \mu_y$), as μ_s increases from 0.1 min^{-1} to 1 min^{-1} . The contribution from the integration sub-motif domi-

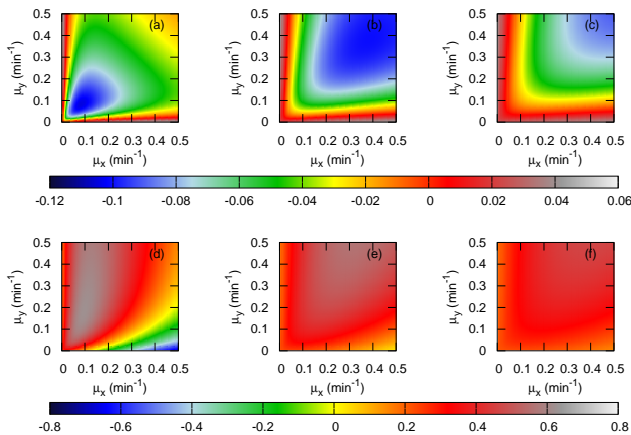


FIG. 6. Panels (a)-(c) depict $\Delta I_{IM-DM}(z; x, y) - \Delta I_{BM-DM}(s; x, y)$ (in bits) as functions of μ_x and μ_y for $\mu_s = 0.1, 0.5$ and, 1 min^{-1} , respectively. Similarly, panels (d)-(f) show $\text{SNR}_{IM-DM} - \text{SNR}_{BM-DM}$ for $\mu_s = 0.1, 0.5$ and, 1 min^{-1} , respectively. SNR_{BM-DM} and SNR_{IM-DM} are computed considering the signaling pathways $S \rightarrow X$ and $X \rightarrow Z$, respectively. The theoretical expressions are obtained using constant populations (at steady state) of the biochemical species: $\langle s \rangle = 10$, $\langle x \rangle = 100$, $\langle y \rangle = 100$ and, $\langle z \rangle = 100$. The expressions for the rate parameters are $k_s = \mu_s \langle s \rangle$, $k_x = \mu_x \langle x \rangle ((K_1^n + \langle s \rangle^n) / \langle s \rangle^n)$, $k_y = \mu_y \langle y \rangle ((K_2^n + \langle s \rangle^n) / \langle s \rangle^n)$ and, $k_z = \mu_z \langle z \rangle ((K_3^n + \langle x \rangle^n) / \langle x \rangle^n) ((K_4^n + \langle y \rangle^n) / \langle y \rangle^n)$. We have kept $K_1 = K_2 = 10$, $K_3 = K_4 = 100$, $\mu_z = 5 \text{ min}^{-1}$ and, $n = 1$ throughout to generate the theoretical profiles.

nates mainly along the region where any one of the tuning parameters (μ_x or μ_y) is small in comparison with its counterpart while the remaining one scans its full range. As μ_s increases, the contribution made by the integration sub-motif also increases thereby encompassing a relatively larger positive domain. The two branches of both bifurcation and integration sub-motifs become identical when X and Y relax identically ($\mu_x = \mu_y$).

In support of the difference in the net synergy shown in Fig. 6(a-c), we now look at the difference in the SNR-s of the sub-motifs. The panels of Fig. 6(d-f), depict the continued variation in the difference between SNR-s of integration and bifurcation sub-motifs i.e., $\text{SNR}_{IM-DM} - \text{SNR}_{BM-DM}$ with μ_s taking values of 0.1 min^{-1} , 0.5 min^{-1} and, 1 min^{-1} , respectively. For computing SNR_{BM-DM} and SNR_{IM-DM} , we have considered the signalling branches $S \rightarrow X$ and $X \rightarrow Z$, respectively. We note that with $\mu_s = 0.1 \text{ min}^{-1}$, the map consists of both positive and negative valued domains. In the positive region, the IM-DM has higher fidelity than the BM-DM whereas, for some specific combinations of the tuning parameters, the BM-DM overpowers the IM-DM, in its efficiency in high fidelity information processing, thereby creating negatively valued region in this map. As μ_s increases, the IM-DM takes control over the entire (μ_x, μ_y) parameter space but the difference between the two SNR-s gradually decreases. This analysis graphically

marks different regions where particular sub-motif plays leading role compared to its counterpart in increasing the fidelity in information transmission.

IV. CONCLUSION

To summarise, we develop an information-theoretic characterisation of DM using the formalism of PID. To know, how much predictive power one biochemical component has about others, we have chosen the metric of net synergy that takes care of synergy, redundancy and, information independence. We have identified two sub-motifs out of the whole motif namely the signal bifurcation motif and the signal integration motif which constitute the DM. Upon writing the corresponding set of Langevin equations, we have utilised LNA and thereafter the steady state version of Lyapunov equation to obtain the analytic expressions for the second moments of the Gaussian random variables representing different biochemical species of the network. The regulatory functions have been chosen, in general, to be nonlinear which is typically the case in real biological systems. In our analysis, we investigate the effect of relaxation time scale on the information transmission in network motifs. It is observed that a slower downstream species fails to sense the faster upstream species and as a consequence, information propagation is hindered in the channel. This study attempts to depict the effect of variation in relaxation time scale in the net synergy landscape lowering redundancy whenever upstream species fluctuates on a faster time scale compared to the downstream species. Our study also reveals the physical reason behind the creation of redundancy in the net synergy profile. We observe only positive net synergy in the integration motif whose two signal integrating branches are architecturally disjoint from above i.e., having no common source of fluctuations. Therefore, we are led to conclude that redundancy arises out of information sharing between different target nodes of the network, caused by a common source of fluctuations. There are indications emanating from variations of the net synergy as a function of various activation coefficients, that biological motifs with better noise handling capabilities, will avoid superactivation and preferentially act within the range of weak and moderate activation level. Efforts were made to quantify the relative information processing strengths of the two sub-motifs of the diamond pattern operating under low, medium and, high relaxation frequency of the signal. The related maps portraying the interplay of SNR-s of the two sub-motifs, under similar parametric conditions in the (μ_x, μ_y) domain, help us to identify regions where specific sub-motifs contribute more towards high fidelity information transmission.

In a nutshell, identifying connection between emergence of synergy and redundancy and, the architectural or topological features of the diamond motif and its sub-motifs, through quantification of the net synergy, forms

the basis of our information-theoretic study. The generalised analysis executed here employing biologically relevant model and parameters, presents key concepts adding novelty to the current understanding of information processing in a diamond motif. This information theory centred framework as presented in this communication, has enormous scope to reveal novel findings in other abundant network motifs, eventually leading towards discovery of some unifying physical principles governing diversified biological systems constituted across length scales and operating across time scales.

ACKNOWLEDGMENTS

Ayan Biswas is thankful to Bose Institute, Kolkata for research fellowship. Financial support from Council of Scientific and Industrial Research (CSIR), India [01(2771)/14/EMR-II] is thankfully acknowledged.

Appendix A: The bifurcation motif

For a bifurcation motif, one needs to consider the dynamics of only S, X and, Y as expressed with the following set of Langevin equations

$$\begin{aligned}\frac{ds}{dt} &= f_s(s) - \mu_s s + \xi_s(t), \\ \frac{dx}{dt} &= f_x(s, x) - \mu_x x + \xi_x(t), \\ \frac{dy}{dt} &= f_y(s, y) - \mu_y y + \xi_y(t).\end{aligned}$$

The corresponding Jacobian obtained from linearizing this set is as follows:

$$\mathbf{J} = \begin{pmatrix} f'_{s,s} - \mu_s & 0 & 0 \\ f'_{x,s} & f'_{x,x} - \mu_x & 0 \\ f'_{y,s} & 0 & f'_{y,y} - \mu_y \end{pmatrix},$$

where $f'_{s,s} \equiv f'_{s,s}(\langle s \rangle)$, $f'_{x,s} \equiv f'_{x,s}(\langle s \rangle, \langle x \rangle)$, $f'_{x,x} \equiv f'_{x,x}(\langle s \rangle, \langle x \rangle)$, $f'_{y,s} \equiv f'_{y,s}(\langle s \rangle, \langle y \rangle)$ and, $f'_{y,y} \equiv f'_{y,y}(\langle s \rangle, \langle y \rangle)$. Here, $\langle \dots \rangle$ denotes steady state ensemble average and $f'_{s,s}(\langle s \rangle)$ symbolically means that the regulatory function f_s has been differentiated with respect to s and evaluated at $\langle s \rangle$, and so on. Using the Jacobian we solve the Lyapunov equation (6) and derive the analytic expressions for variance and covariance associated with

the bifurcation motif.

$$\Sigma(s) = \frac{\alpha_s}{2(\mu_s - f'_{s,s})}, \quad (\text{A1})$$

$$\Sigma(s, x) = \frac{f'_{x,s} \Sigma(s)}{(\mu_s - f'_{s,s}) + (\mu_x - f'_{x,x})}, \quad (\text{A2})$$

$$\Sigma(s, y) = \frac{f'_{y,s} \Sigma(s)}{(\mu_s - f'_{s,s}) + (\mu_y - f'_{y,y})}, \quad (\text{A3})$$

$$\Sigma(x) = \frac{\alpha_x}{2(\mu_x - f'_{x,x})} + \frac{f'_{x,s} \Sigma(s, x)}{(\mu_x - f'_{x,x})}, \quad (\text{A4})$$

$$\Sigma(y) = \frac{\alpha_y}{2(\mu_y - f'_{y,y})} + \frac{f'_{y,s} \Sigma(s, y)}{(\mu_y - f'_{y,y})}, \quad (\text{A5})$$

$$\Sigma(x, y) = \frac{f'_{y,s} \Sigma(s, x) + f'_{x,s} \Sigma(s, y)}{(\mu_x - f'_{x,x}) + (\mu_y - f'_{y,y})}. \quad (\text{A6})$$

In our calculation, we have used $f_s = k_s$, $f_x = k_x(s^n/(K_1^n + s^n))$ and, $f_y = k_y(s^n/(K_2^n + s^n))$. $\alpha_i \equiv \langle |\xi_i|^2 \rangle$ ($i = s, x, y$) imply the ensemble averaged noise strengths evaluated at steady state.

Appendix B: The integration motif

For the integration motif, only species X, Y and, Z are taken into account for which the Langevin description stands like the following:

$$\begin{aligned}\frac{dx}{dt} &= f_x(x) - \mu_x x + \xi_x(t), \\ \frac{dy}{dt} &= f_y(y) - \mu_y y + \xi_y(t), \\ \frac{dz}{dt} &= f_z(x, y, z) - \mu_z z + \xi_z(t).\end{aligned}$$

with the Jacobian,

$$\mathbf{J} = \begin{pmatrix} f'_{x,x} - \mu_x & 0 & 0 \\ 0 & f'_{y,y} - \mu_y & 0 \\ f'_{z,x} & f'_{z,y} & f'_{z,z} - \mu_z \end{pmatrix}.$$

Here $f'_{x,x} \equiv f'_{x,x}(\langle x \rangle)$, $f'_{y,y} \equiv f'_{y,y}(\langle y \rangle)$, $f'_{z,x} \equiv f'_{z,x}(\langle x \rangle, \langle y \rangle, \langle z \rangle)$, $f'_{z,y} \equiv f'_{z,y}(\langle x \rangle, \langle y \rangle, \langle z \rangle)$ and, $f'_{z,z} \equiv f'_{z,z}(\langle x \rangle, \langle y \rangle, \langle z \rangle)$. As in the previous case $\langle \dots \rangle$ denotes steady state ensemble average and $f'_{x,x}(\langle x \rangle)$ symbolically means that the regulatory function f_x has been differentiated with respect to x and evaluated at $\langle x \rangle$, and so on. Solving the corresponding Lyapunov equation (6) at

steady state yields expressions of the second moments,

$$\Sigma(x) = \frac{\alpha_x}{2(\mu_x - f'_{x,x})}, \quad (\text{B1})$$

$$\Sigma(y) = \frac{\alpha_y}{2(\mu_y - f'_{y,y})}, \quad (\text{B2})$$

$$\Sigma(x, y) = 0, \quad (\text{B3})$$

$$\Sigma(x, z) = \frac{f'_{z,x} \Sigma(x)}{(\mu_x - f'_{x,x}) + (\mu_z - f'_{z,z})}, \quad (\text{B4})$$

$$\Sigma(y, z) = \frac{f'_{z,y} \Sigma(y)}{(\mu_y - f'_{y,y}) + (\mu_z - f'_{z,z})}, \quad (\text{B5})$$

$$\Sigma(z) = \frac{\alpha_z}{2(\mu_z - f'_{z,z})} + \frac{f'_{z,x} \Sigma(x, z) + f'_{z,y} \Sigma(y, z)}{(\mu_z - f'_{z,z})}. \quad (\text{B6})$$

Here, $f_x = k_x$, $f_y = k_y$, $f_z = k_z(x^n/(K_3^n + x^n))(y^n/(K_4^n + y^n))$ and, α_i -s ($i = x, y, z$) imply, as in the previous case, steady state ensemble averaged noise strengths of different biochemical species.

Appendix C: The diamond motif

For a diamond motif, where S, X, Y and, Z are all involved, the full set of Langevin equations are

$$\begin{aligned} \frac{ds}{dt} &= f_s(s) - \mu_s s + \xi_s(t), \\ \frac{dx}{dt} &= f_x(s, x) - \mu_x x + \xi_x(t), \\ \frac{dy}{dt} &= f_y(s, y) - \mu_y y + \xi_y(t), \\ \frac{dz}{dt} &= f_z(s, x, y, z) - \mu_z z + \xi_z(t). \end{aligned}$$

For the above mentioned kinetics the Jacobian becomes

$$\mathbf{J} = \begin{pmatrix} f'_{s,s} - \mu_s & 0 & 0 & 0 \\ f'_{x,s} & f'_{x,x} - \mu_x & 0 & 0 \\ f'_{y,s} & 0 & f'_{y,y} - \mu_y & 0 \\ f'_{z,s} & f'_{z,x} & f'_{z,y} & f'_{z,z} - \mu_z \end{pmatrix}.$$

Here, $f'_{s,s} \equiv f'_{s,s}(\langle s \rangle)$, $f'_{x,s} \equiv f'_{x,s}(\langle s \rangle, \langle x \rangle)$, $f'_{x,x} \equiv f'_{x,x}(\langle s \rangle, \langle x \rangle)$, $f'_{y,s} \equiv f'_{y,s}(\langle s \rangle, \langle y \rangle)$, $f'_{y,y} \equiv$

$f'_{y,y}(\langle s \rangle, \langle y \rangle)$, $f'_{z,s} \equiv f'_{z,s}(\langle s \rangle, \langle x \rangle, \langle y \rangle, \langle z \rangle)$, $f'_{z,x} \equiv f'_{z,x}(\langle s \rangle, \langle x \rangle, \langle y \rangle, \langle z \rangle)$, $f'_{z,y} \equiv f'_{z,y}(\langle s \rangle, \langle x \rangle, \langle y \rangle, \langle z \rangle)$ and, $f'_{z,z} \equiv f'_{z,z}(\langle s \rangle, \langle x \rangle, \langle y \rangle, \langle z \rangle)$. The notations $\langle \dots \rangle$, $f'_{s,s}(\langle s \rangle)$, etc. have the usual meaning as mentioned in the previous two cases. Again with the help of the Lyapunov equation (6), we get the following analytic expressions for variance and covariance,

$$\Sigma(s) = \frac{\alpha_s}{2(\mu_s - f'_{s,s})}, \quad (\text{C1})$$

$$\Sigma(s, x) = \frac{f'_{x,s} \Sigma(s)}{(\mu_s - f'_{s,s}) + (\mu_x - f'_{x,x})}, \quad (\text{C2})$$

$$\Sigma(s, y) = \frac{f'_{y,s} \Sigma(s)}{(\mu_s - f'_{s,s}) + (\mu_y - f'_{y,y})}, \quad (\text{C3})$$

$$\Sigma(s, z) = \frac{f'_{z,s} \Sigma(s) + f'_{z,x} \Sigma(s, x) + f'_{z,y} \Sigma(s, y)}{(\mu_s - f'_{s,s}) + (\mu_z - f'_{z,z})}, \quad (\text{C4})$$

$$\Sigma(x) = \frac{\alpha_x}{2(\mu_x - f'_{x,x})} + \frac{f'_{x,s} \Sigma(s, x)}{(\mu_x - f'_{x,x})}, \quad (\text{C5})$$

$$\Sigma(y) = \frac{\alpha_y}{2(\mu_y - f'_{y,y})} + \frac{f'_{y,s} \Sigma(s, y)}{(\mu_y - f'_{y,y})}, \quad (\text{C6})$$

$$\Sigma(x, y) = \frac{f'_{x,s} \Sigma(s, y) + f'_{y,s} \Sigma(s, x)}{(\mu_x - f'_{x,x}) + (\mu_y - f'_{y,y})}, \quad (\text{C7})$$

$$\Sigma(x, z) = \frac{f'_{x,s} \Sigma(s, z) + f'_{z,s} \Sigma(s, x) + f'_{z,x} \Sigma(x) + f'_{z,y} \Sigma(x, y)}{(\mu_x - f'_{x,x}) + (\mu_z - f'_{z,z})}, \quad (\text{C8})$$

$$\Sigma(y, z) = \frac{f'_{y,s} \Sigma(s, z) + f'_{z,s} \Sigma(s, y) + f'_{z,y} \Sigma(y) + f'_{z,x} \Sigma(x, y)}{(\mu_y - f'_{y,y}) + (\mu_z - f'_{z,z})}, \quad (\text{C9})$$

$$\Sigma(z) = \frac{\alpha_z}{2(\mu_z - f'_{z,z})} + \frac{f'_{z,s} \Sigma(s, z) + f'_{z,x} \Sigma(x, z) + f'_{z,y} \Sigma(y, z)}{(\mu_z - f'_{z,z})}. \quad (\text{C10})$$

For diamond motif, the regulatory functions are chosen as, $f_s = k_s$, $f_x = k_x(s^n/(K_1^n + s^n))$, $f_y = k_y(s^n/(K_2^n + s^n))$, $f_z = k_z(x^n/(K_3^n + x^n))(y^n/(K_4^n + y^n))$ and α_i -s ($i = s, x, y, z$) stand for different steady state noise strengths obtained through ensemble averaging. We utilize these expressions of second moments (Eqs. C1-C10) to compute $\Delta I_{BM-DM}(s; x, y)$ and $\Delta I_{IM-DM}(z; x, y)$, as required.

-
- [1] M. Thattai and A. van Oudenaarden, Proc. Natl. Acad. Sci. U.S.A. **98**, 8614 (2001).
 [2] H. B. Fraser, A. E. Hirsh, G. Giaever, J. Kumm, and M. B. Eisen, PLoS Biol. **2**, e137 (2004).
 [3] C. T. Bergstrom and M. Lachmann, *Shannon information and biological fitness in Information Theory Work-*

- shop* (IEEE, 2004).
 [4] W. Bialek and S. Setayeshgar, Proc. Natl. Acad. Sci. U.S.A. **102**, 10040 (2005).
 [5] B. Ghosh, R. Karmakar, and I. Bose, Phys Biol **2**, 36 (2005).
 [6] W. Bialek and S. Setayeshgar, Phys. Rev. Lett. **100**,

- 258101 (2008).
- [7] G. Tkačik, C. G. Callan, and W. Bialek, *Phys Rev E* **78**, 011910 (2008).
- [8] W. Bialek, *Biophysics: Searching for principles* (Princeton University Press, Princeton, 2012).
- [9] C. G. Bowsher and P. S. Swain, *Curr. Opin. Biotechnol.* **28**, 149 (2014).
- [10] A. Levchenko and I. Nemenman, *Curr. Opin. Biotechnol.* **28**, 156 (2014).
- [11] S. S. Mc Mahon, A. Sim, S. Filippi, R. Johnson, J. Liepe, D. Smith, and M. P. Stumpf, *Semin. Cell Dev. Biol.* **35**, 98 (2014).
- [12] J. Selimkhanov, B. Taylor, J. Yao, A. Pilko, J. Albeck, A. Hoffmann, L. Tsimring, and R. Wollman, *Science* **346**, 1370 (2014).
- [13] D. Hathcock, J. Sheehy, C. Weisenberger, E. Ilker, and M. Hinczewski, *IEEE Transactions on Molecular, Biological and Multi-Scale Communications* **2**, 16 (2016).
- [14] C. E. Shannon, *Bell. Syst. Tech. J* **27**, 379 (1948).
- [15] T. M. Cover and J. A. Thomas, *Elements of Information Theory* (Wiley-Interscience, New York, 1991).
- [16] A. Borst and F. E. Theunissen, *Nat. Neurosci.* **2**, 947 (1999).
- [17] P. P. Mitra and J. B. Stark, *Nature* **411**, 1027 (2001).
- [18] E. Ziv, I. Nemenman, and C. H. Wiggins, *PLoS ONE* **2**, e1077 (2007).
- [19] I. Lestas, G. Vinnicombe, and J. Paulsson, *Nature* **467**, 174 (2010).
- [20] F. Tostevin and P. R. ten Wolde, *Phys. Rev. E* **81**, 061917 (2010).
- [21] R. Cheong, A. Rhee, C. J. Wang, I. Nemenman, and A. Levchenko, *Science* **334**, 354 (2011).
- [22] G. Tkačik and A. M. Walczak, *J. Phys. Condens. Matter* **23**, 153102 (2011).
- [23] A. Rhee, R. Cheong, and A. Levchenko, *Phys Biol* **9**, 045011 (2012).
- [24] C. G. Bowsher, M. Voliotis, and P. S. Swain, *PLoS Comput. Biol.* **9**, e1002965 (2013).
- [25] L. S. Tsimring, *Rep. Prog. Phys.* **77**, 026601 (2014).
- [26] A. S. Hansen and E. K. O'Shea, *Elife* **4**, e06559 (2015).
- [27] R. Milo, S. Shen-Orr, S. Itzkovitz, N. Kashtan, D. Chklovskii, and U. Alon, *Science* **298**, 824 (2002).
- [28] F. Mancini, C. H. Wiggins, M. Marsili, and A. M. Walczak, *Phys. Rev. E* **88**, 022708 (2013).
- [29] W. Weaver, *Sci. Am.* **181**, 11 (1949).
- [30] U. Alon, *An Introduction to Systems Biology: Design Principles of Biological Circuits* (CRC Press, Boca Raton, 2006).
- [31] U. Alon, *Nat. Rev. Genet.* **8**, 450 (2007).
- [32] W. H. de Ronde, F. Tostevin, and P. R. ten Wolde, *Phys Rev E* **86**, 021913 (2012).
- [33] A. Cournac and J. A. Sepulchre, *BMC Syst Biol* **3**, 29 (2009).
- [34] E. Schneidman, W. Bialek, and M. J. Berry, *J. Neurosci.* **23**, 11539 (2003).
- [35] A. B. Barrett, *Phys. Rev. E* **91**, 052802 (2015).
- [36] P. L. Williams and R. D. Beer (2010), arXiv:cs.IT/1004.2515.
- [37] L. Faes, D. Kugiumtzis, G. Nollo, F. Jurysta, and D. Marinazzo, *Phys Rev E* **91**, 032904 (2015).
- [38] L. Faes, A. Porta, G. Nollo, and M. Javorka, *Entropy* **19**, 5 (2017).
- [39] L. Faes, A. Porta, and G. Nollo, *Entropy* **17**, 277 (2015).
- [40] N. Bertschinger, J. Rauh, E. Olbrich, J. Jost, and N. Ay, *Entropy* **16**, 2161 (2014).
- [41] V. Griffith and C. Koch, in *Guided self-organization: Inception, Emergence, complexity and computation*, edited by M. Prokopenko (Springer, Berlin, 2014), vol. 9, pp. 159–190.
- [42] M. Harder, C. Salge, and D. Polani, *Phys Rev E* **87**, 012130 (2013).
- [43] M. Wibral, V. Priesemann, J. W. Kay, J. T. Lizier, and W. A. Phillips, *Brain Cogn* **112**, 25 (2017).
- [44] T. J. Gawne and B. J. Richmond, *J. Neurosci.* **13**, 2758 (1993).
- [45] S. Panzeri, S. R. Schultz, A. Treves, and E. T. Rolls, *Proc. Biol. Sci.* **266**, 1001 (1999).
- [46] N. Brenner, S. P. Strong, R. Koberle, W. Bialek, and R. R. de Ruyter van Steveninck, *Neural Comput* **12**, 1531 (2000).
- [47] C. E. Shannon and W. Weaver, *The mathematical theory of communication* (Urbana: University of Illinois Press, 1963).
- [48] A. Biswas and S. K. Banik, *Phys Rev E* **93**, 052422 (2016).
- [49] G. Tkačik, A. M. Walczak, and W. Bialek, *Phys Rev E* **80**, 031920 (2009).
- [50] G. Rodrigo and J. F. Poyatos, *PLoS Comput. Biol.* **12**, e1005156 (2016).
- [51] A. Rhee, R. Cheong, and A. Levchenko, *Proc. Natl. Acad. Sci. U.S.A.* **111**, 17330 (2014).
- [52] F. J. Bruggeman, N. Blüthgen, and H. V. Westerhoff, *PLoS Comput. Biol.* **5**, e1000506 (2009).
- [53] M. Hinczewski and D. Thirumalai, *Phys. Rev. X* **4**, 041017 (2014).
- [54] A. K. Maity, P. Chaudhury, and S. K. Banik, *PLoS ONE* **10**, e0123242 (2015).
- [55] W. H. de Ronde, F. Tostevin, and P. R. ten Wolde, *Phys. Rev. E* **82**, 031914 (2010).
- [56] S. Tănase-Nicola, P. B. Warren, and P. R. ten Wolde, *Phys. Rev. Lett.* **97**, 068102 (2006).
- [57] P. B. Warren, S. Tănase-Nicola, and P. R. ten Wolde, *J. Chem. Phys.* **125**, 144904 (2006).
- [58] A. K. Maity, A. Bandyopadhyay, P. Chaudhury, and S. K. Banik, *Phys. Rev. E* **89**, 032713 (2014).
- [59] R. Grima, *Phys. Rev. E* **92**, 042124 (2015).
- [60] M. B. Elowitz, A. J. Levine, E. D. Siggia, and P. S. Swain, *Science* **297**, 1183 (2002).
- [61] J. Paulsson, *Nature* **427**, 415 (2004).
- [62] J. Elf and M. Ehrenberg, *Genome Res.* **13**, 2475 (2003).
- [63] N. G. van Kampen, *Stochastic Processes in Physics and Chemistry, 3rd ed.* (North-Holland, Amsterdam, 2007).
- [64] F. Tostevin and P. R. ten Wolde, *Phys. Rev. Lett.* **102**, 218101 (2009).
- [65] L. Bintu, N. E. Buchler, H. G. Garcia, U. Gerland, T. Hwa, J. Kondev, and R. Phillips, *Curr. Opin. Genet. Dev.* **15**, 116 (2005).
- [66] G. Tkačik, T. Gregor, and W. Bialek, *PLoS ONE* **3**, e2774 (2008).
- [67] A. M. Walczak, G. Tkačik, and W. Bialek, *Phys Rev E* **81**, 041905 (2010).
- [68] G. Tkačik, C. G. Callan, and W. Bialek, *Proc. Natl. Acad. Sci. U.S.A.* **105**, 12265 (2008).
- [69] D. T. Gillespie, *J. Comp. Phys.* **22**, 403 (1976).
- [70] D. T. Gillespie, *J. Phys. Chem.* **81**, 2340 (1977).
- [71] P. S. Swain, *J. Mol. Biol.* **344**, 965 (2004).
- [72] P. Mehta, S. Goyal, and N. S. Wingreen, *Mol. Syst. Biol.* **4**, 221 (2008).

- [73] J. Keizer, *Statistical Thermodynamics of Nonequilibrium Processes* (Springer-Verlag, Berlin, 1987).
- [74] J. Paulsson, *Phys Life Rev* **2**, 157 (2005).